Available online at www.sciencedirect.com

ScienceDirect

Ceramics International 40 (2014) 5055–5059

CERAMICS INTERNATIONAL

www.elsevier.com/locate/ceramint

Short communication

Graphene spheres loaded urchin-like Cu_xO ($x=1$ or 2) for use as a high performance photocatalyst

Bin Zeng, Xiaohua Chen*, Youxin Luo, Qiyuan Liu, Wujun Zeng

College of Mechanical Engineering, Hunan University of Arts and Science, Changde 415000, People's Republic of China

Received 30 July 2013; received in revised form 5 September 2013; accepted 5 September 2013
Available online 25 September 2013

Abstract

Graphene sphere decorated with urchin-like CuO and Cu_2O (Cu_xO, $x=1$ or 2) was successfully synthesized by spray drying and post-calcinating method. Scanning electron microscopy and transmission electron microscopy observations confirmed that graphene formed a spherical micrometer structure and urchin-like Cu_xO were decorated on their surface. The experimental results indicated that these novel nanocomposites showed excellent photocatalytic performance in the presence of H_2O_2 under visible light. This could be attributed to a fast and long-distance electron transport in one-dimensional geometry and an effective separation of photogenerated electron–hole pairs for an intimate interfacial contact between Cu_xO and graphene sphere.

Keywords: Graphene; Spray drying; Photocatalytic performance

1. Introduction

Cu_xO with narrow band gaps (1.2 eV and 2.0 eV) has been widely exploited for photocatalysts [1], lithium ion electrode material [2] and optical switches [3]. In recent years, Cu_xO nanostructures in the form of one-dimensional, two-dimensional and three-dimensional structures have been largely studied [4–6]. Among them, one-dimensional (1D) structure acts as an alternative nanophotocatalyst and has been proved to be beneficial to the photocatalytic activity for the following advantages. First, the 1D geometry leads to a fast and long-distance electron transport. Second, the light absorption and scattering can be obviously enhanced because of the high length-to-diameter ratio of the 1D structure. Lastly, 1D structure is expected to have larger specific surface area compared to the particle counterparts [7].

In the past several years, graphene has drawn much attention for its unique atom-thick 2D structure, high specific surface area, superior electron mobility and electrochemical stability [8]. Numerous studies have demonstrated that assembling nanomaterials on graphene sheets can exhibit excellent photocatalytic performance and it is ascribed to the following two reasons. One is that the two-dimensional (2D) platform structure makes it an excellent supporting matrix for photocatalyst particles. The other is that the graphene with excellent electronic conductivity can effectively inhibit the recombination of the electron–hole pairs in the nanocomposites [9].

Herein, we successfully synthesized graphene sphere loaded urchin-like Cu_xO (GR–Cu_xO) as an efficient visible light photocatalytic material by spray drying and post-calcinating method. The experimental results revealed that these novel nanostructures exhibited much higher visible light photocatalytic activities for MO dye degradation.

2. Experimental details

Graphite oxide (GO) was prepared using Hummers method [10]. In a typical synthesis process, 3 g of graphite powder and 3 g of sodium nitrate were put into 150 ml of H_2SO_4 (in an ice bath). Afterward, 9 g of $KMnO_4$ was gradually added. The mixture was then transferred to 40 °C water bath and stirred for about 2 h, forming a thick paste. Subsequently, 150 ml of deionized water was added gradually and increased the temperature to 98 °C. After

*Corresponding author. Tel.: +86 732 6624382.
E-mail address: 21467855@qq.com (X. Chen).

0272-8842/$ - see front matter © 2013 Elsevier Ltd and Techna Group S.r.l. All rights reserved.
http://dx.doi.org/10.1016/j.ceramint.2013.09.021

20 min, 30 ml of 35% H_2O_2 solution was added to the mixture. The mixture was stirred for another 10 min and then diluted with 1000 ml of deionized water. The solution was then filtered and washed with de-ionized water until the pH was 7.

The synthesis of GR–Cu_xO was as follows: 50 ml of 20 g L^{-1} copper acetate ($Cu(AC)_2$) was added to 30 ml of 1 g L^{-1} graphene oxides (GO) solution. After sonication for 30 min the blended suspension was spray-dried at 210 °C and a blue powder was obtained. Next the obtained powder was calcinated at 220 °C for 2 h (thermal decomposition of Cu $(AC)_2$) and then sintered at 800 °C for 2 h (reduction of GO) under argon atmosphere in a tube furnace. Finally, they were allowed to cool down to 300 °C to hold for 3 h under an air atmosphere (oxidation of decomposed product). For comparison, the same method was used to synthesize Cu_xO without GO and graphene spheres without $Cu(AC)_2$.

The characterization of the as-prepared product was carried out by scanning electron microscopy and energy dispersive spectrometer (SEM, S4800), transmission electron microscopy (TEM, JEM-2100 F), powder x-ray diffraction (XRD, D5000), and Raman spectra (J-Y, T6400).

The photocatalytic degradation of methyl orange (MO) was measured at ambient temperature in the presence of H_2O_2. 20 mg as-products were dispersed in 300 ml MO solution of 20 mg L^{-1}, to which 2 mL of H_2O_2 was added. It was placed beside the beaker at a distance of 20 cm. After stirring for 30 min in darkness 500 W xenon arc lamp was used as a light source. A 5 ml portion was then removed every 5 min and was centrifuged immediately to separate the suspended solid. The absorbance of the supernate at 464 nm was analyzed by UV–vis spectrophotometry.

3. Results and discussion

The XRD taken from as-prepared products is shown in Fig. 1. The peaks at 35.6°, 38.8°, 48.89° and 61.6° can be assigned to (002), (111), (−202) and (−113) crystal planes of CuO, respectively (JCPDS no. 41-0254). The peaks at 38.2°, 42.4° and 73.7° correspond well to the (111), (200) and (311) crystal planes of Cu_2O, respectively (JCPDS no. 78-2076). An evident peak at the 2θ value of about 25.3° accounts for the reflection of graphene (002) plane [11]. From the XRD patterns, no other characteristic peaks corresponding to any impurity are obtained.

The formation of GR–Cu_xO is further confirmed from the Raman spectra (Fig. 2). It is seen that GO exhibits a D band at 1331 cm^{-1}, arising from the disruption of the symmetrical hexagonal graphitic lattice, and a G band at 1585 cm^{-1}, arising from the response of the in-plane stretching motion of symmetric sp^2 C–C bonds. For GR–Cu_xO the corresponding band is at 1325 and 1568 cm^{-1}. Obviously a blue shift of D and G band is observed and this might result from the recovery of the hexagonal network of carbon atom in graphene [12]. The D/G intensity ratio for GO is 1.03, however, this value increases to 1.11 for GR–Cu_xO. The increase of D/G ratio indicates a formation of new graphitic domains after thermal treatment, indicating a partial reduction from graphene oxides to graphene [11].

Fig. 3a is the SEM of GR–Cu_xO and it shows a spherical morphology with rough appearance. After close observation of this architecture in Fig. 2b and c we can clearly see uniform and discrete urchin-like Cu_xO is spread on the surface of GR spheres. TEM image further indicates that urchin Cu_xO, with about 5 nm in diameter and more than 100 nm in length diffuses and tightly attaches onto the graphene. Detailed structural analysis of single Cu_xO was performed by HRTEM (Fig. 3e) and the size details of the urchin like structure are in accordance with those provided by TEM. The lattice spaces of 0.272 nm and 0.243 nm could be indexed as (110) plane of CuO and (111) plane of Cu_2O, respectively. The selected area electron diffraction (SAED) pattern (Fig. 3f) indicates the polycrystalline nature of nano-urchins Cu_xO. The result indicates that graphene spheres not only provide an ideal substrate for loading urchin-like Cu_xO but also inhibit their aggregation. Furthermore, as previously reported, through electrostatic binding and physisorption, urchin-like Cu_xO could couple with graphene spheres, thus promoting the efficient electron transport properties in GR–Cu_xO.

Based on the experimental results mentioned above, schematic illustrations are presented for the formation of GR–Cu_xO, as shown in Fig. 4. With the addition of $Cu(AC)_2$

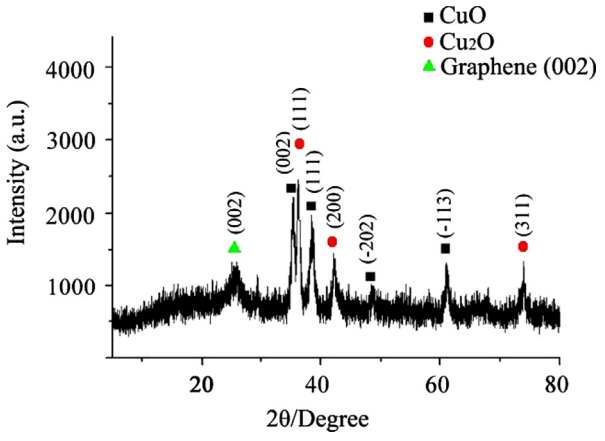

Fig. 1. XRD pattern of GR–Cu_xO.

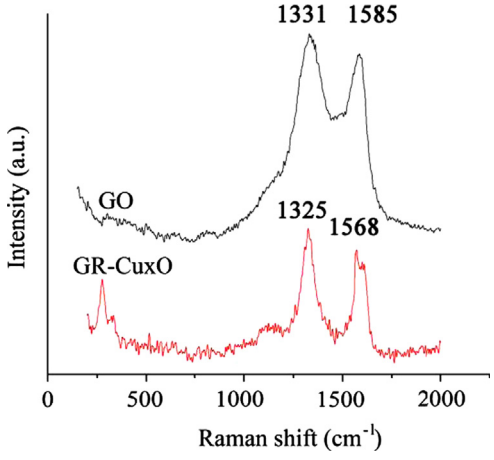

Fig. 2. Raman spectra of GO and GR–Cu_xO.

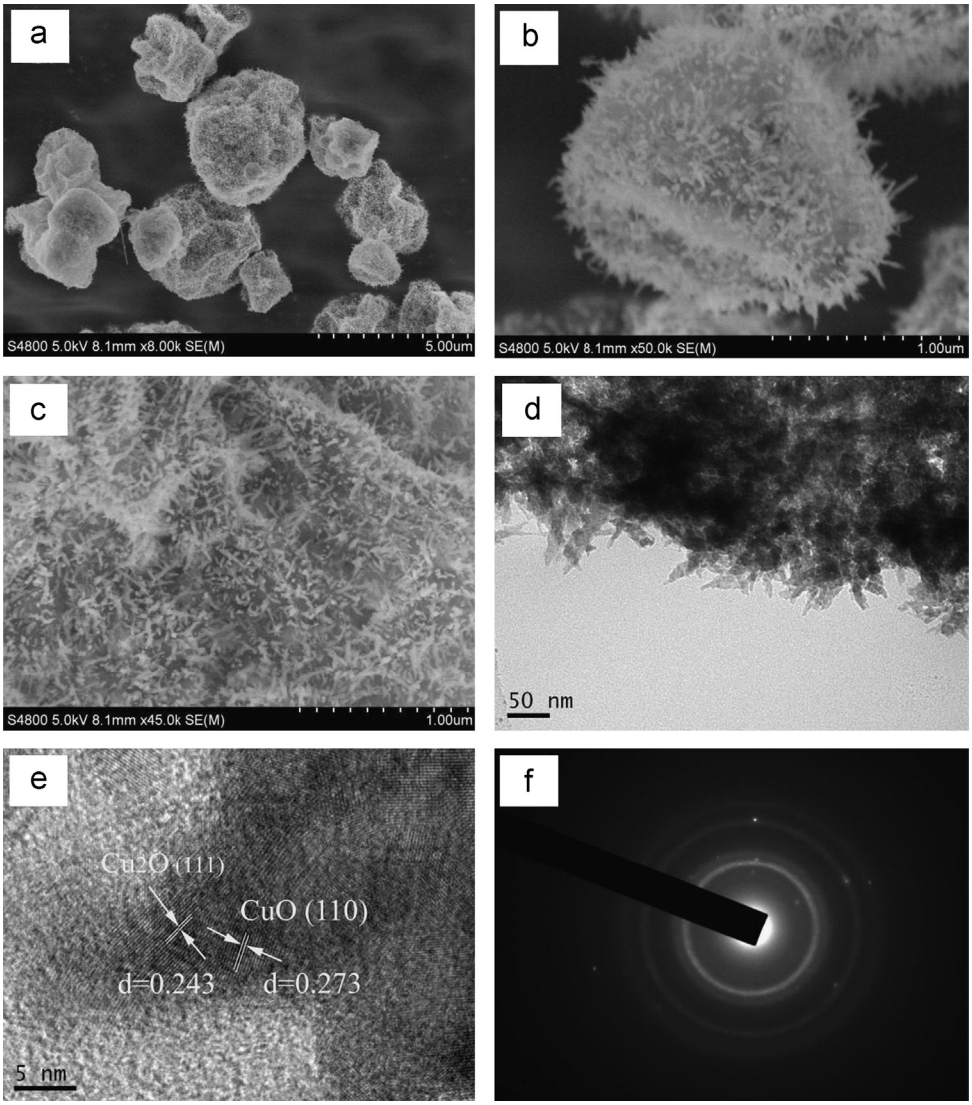

Fig. 3. SEM, TEM, HRTEM and SAED images of GR–Cu_xO (a), (b), (c) SEM, (d) TEM, (e) HRTEM, and (f) SAED.

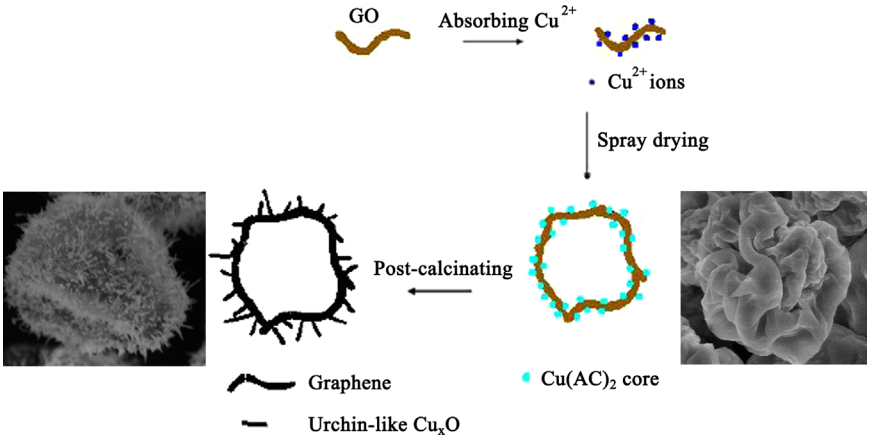

Fig. 4. Proposed scheme of the fabricated processes of GR–Cu_xO.

solution into GO solution with ultrasonication, Cu^{2+} ions are attaching onto the GO surface due to the electrostatic interactions with the functional groups [13]. After spray drying, the maximum structural stability of the solution is in a spherical form, allowing the formation of spherical structure [14], in which $Cu(AC)_2$ particles are attached on the surface of GO spheres. Finally, by a thermal treatment $Cu(AC)_2$ are decomposed to urchin-like Cu_xO and GO are reduced [15].

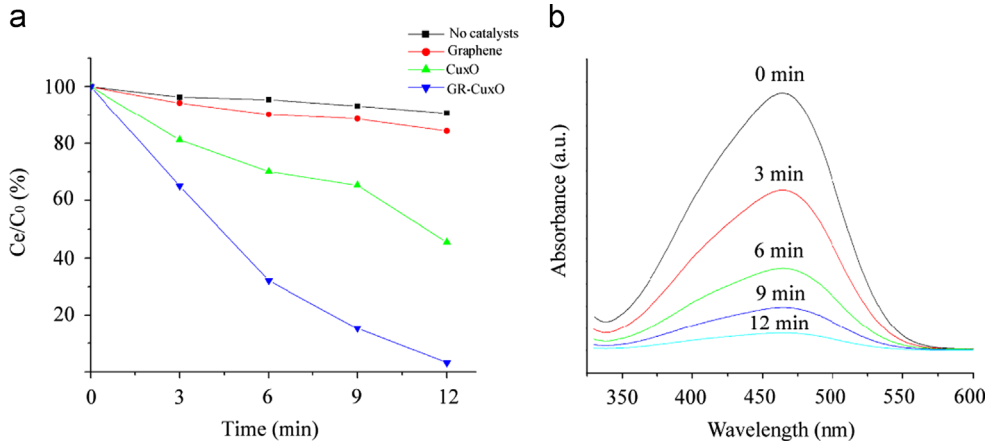

Fig. 5. (a) Photocatalytic degradation efficiency of MO by different catalysts. (b) UV–vis absorption spectra of MO solution with GR–Cu_xO at different time intervals.

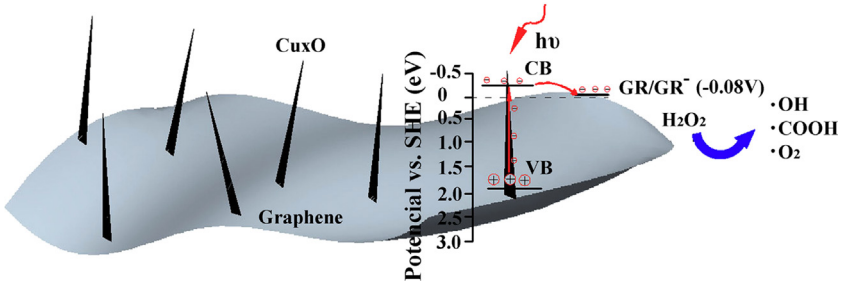

Scheme 1. The proposed mechanism of MO degradation.

As a demonstration of application of GR–Cu_xO, MO is chosen as a representative organic dyestuff to evaluate the photocatalytic performance and the degradation ratio was calculated with (C_e/C_0), where C_0 is the initial concentration and C_e is the concentration of MO at different times. Fig. 5a shows the profile of the photocatalytic degradation efficiency of MO for different catalysts in the presence of H_2O_2. In the absence of catalyst, only a slight degradation (less than 10%) of MO is observed after 12 min irradiation, while about 96.1% of MO is degraded in the presence of GR–Cu_xO. Furthermore, about 16.1% and 56.4% of MO was degraded by graphene and Cu_xO, respectively, indicating an obvious advantage of GR–Cu_xO in their ability to make use of visible light. Fig. 5b shows the typical time-dependent UV–vis absorption spectra of MO solution during the photodegradation in the presence of GR–Cu_xO. It is seen that the absorption peak at 464 nm, corresponding to the MO molecule, weakens gradually as the exposure time increases and nearly disappears after 12 min.

The high catalytic performance of the GR–Cu_xO nanocomposites can be explained from Scheme 1. Under UV–vis illumination, electrons are excited from the valence band (VB) to the conduction band (CB) inside the one-dimensional structure and these charge carriers recombine easily resulting in a low photocatalytic performance [16]. When nanoparticles are immobilized on the surface of graphene sphere, the photogenerated electrons in CB of Cu_xO tend to transfer to graphene sphere, leading to the hole–electron separation [17]. Furthermore, since the potential of graphene/graphene$^-$ (GR/GR$^-$) is about -0.08 V (vs SHE, pH $=0$) [18], it can act as a cocatalyst to promote the separation and transfer of photogenerated electrons from CB of Cu_xO to the rGO, consequently improving the photocatalytic reaction. Meanwhile, for MO molecules with aromatic structure, the electrostatic interaction and $\pi-\pi$ conjugation interaction with GR can effectively host both Cu_xO and MO molecules. When electron donor and acceptor molecules come to a close proximity, the electron transfer process is facilitated, resulting in an improved photodegradation activity [19]. Finally, •OH radicals generated from the reduction of H_2O_2 by the photo-generated electrons directly decompose the pollutant dye [20].

4. Conclusions

In this paper, we prepared graphene spherical structure decorated with urchin-like Cu_xO by spray-drying and post-calcinating method for the first time. Photocatalytic performance shows that GR-Cu_xO spherical structure increases considerably the rate of MO degradation. The present study provides a low-cost, convenient method for assembling various graphene-based composites in applications of water purification as well as optoelectronic fields at a large scale.

Acknowledgments

This work was supported by the Construct Program of the Key Discipline in Hunan Province (XJF[2011] 76) and

General Project of Hunan Provincial Education Department (11C0910).

References

[1] D. Barreca, et al., ChemSusChem 2 (2009) 230–233.
[2] J.C. Park, J. Kim, H. Kwon, H. Song, Advanced Materials 21 (2009) 803–807.
[3] B.J. Hansen, et al., Journal of Physical Chemistry C 114 (2010) 2440–2447.
[4] C. Li, et al., Solid State Communications 150 (2010) 585–589.
[5] L. Wang, et al., Applied Surface Science 271 (2013) 136–140.
[6] L.C. Jiang, W.D. Zhang, Biosensors and Bioelectronics 25 (2010) 1402–1407.
[7] S. Liu, N. Zhang, Z.R. Tang, Y.J. Xu, ACS Applied Materials and Interfaces 4 (2012) 6378–6385.
[8] Q. Xiang, J. Yu, M. Jaroniec, Chemical Society Reviews 41 (2012) 782–796.
[9] S. Bai, X. Shen, RSC Advances 2 (2012) 64–98.
[10] W.S. Hummers Jr., R.E. Offeman, Journal of the American Chemical Society 80 (1958) (1339–1339).
[11] Y. Zhang, et al., Catalysis Science and Technology 1 (2011) 1636–1640.
[12] Y. Zhang, et al., Langmuir 28 (2012) 12893–12900.
[13] Z.H. Huang, et al., Langmuir 27 (2011) 7558–7562.
[14] A. Alhalaweh, S.P. Velaga, Crystal Growth and Design 10 (2010) 3302–3305.
[15] S. Mao, G. Lu, K. Yu, Z. Bo, J. Chen, Advanced Materials 22 (2010) 3521–3526.
[16] Z. Wang, S. Zhao, S. Zhu, Y. Sun, M. Fang, Crystal Engineering Communication 13 (2011) 2262–2267.
[17] X.Y. Yan, et al., Chemical Communications 48 (2012) 1892–1894.
[18] Jun Zhang, Jiaguo Yu, Mietek Jaroniec, Jian Ru Gong, Nano Letters 12 (2012) 4584–4589.
[19] Abhinandan Makhal, Soumik Sarkar, Samir Kumar Pal, Inorganic Chemistry 51 (2012) 10203–10210.
[20] B. Zeng, et al., Applied Surface Science 276 (2013) 482–486.